Program Digest, 2019 IEEE International Ultrasonics Symposium (IUS)
Glasgow, Scotland, October 6-9, 2019

Quantification of Noise in Shear Wave Elasticity Imaging Caused by Speckle

Thomas Ersepke, Tim C. Kranemann, and Georg Schmitz

Chair for Medical Engineering, Ruhr University Bochum, Bochum, Germany
{thomas.ersepke, tim.kranemann, georg.schmitz}@rub.de

***Abstract*—In time-of-flight shear wave elasticity imaging (SWEI), shear wave arrival times at laterally offset tracking positions are used for the reconstruction of the shear wave speed (SWS). Typically, regression filters along the lateral direction are used to smooth the noisy differential arrival times or, if divided by the tracking distance, the noisy shear wave slowness estimates. A major source of error in SWEI is based on the underlying speckle pattern. Thereby, the tracking position can be biased towards constructive interference of randomly distributed scatterers. Since the speckle effect is closely related to the parameters of the ultrasound imaging system, the quality of the SWS images depends on these parameters. In this contribution, the relationship between the variance of the slowness estimates and parameters such as the lateral and axial dimensions of the imaging point spread function, the segment length of the displacement estimation scheme, the lateral tracking distance and the impact of the actual shear wave speed was quantified through numerical simulations. The results provide a basis for an improved understanding of how speckle corrupts the SWS estimation.**

***Index Terms*—Elastography, shear wave imaging, speckle, noise, point spread function**

I. Introduction

Shear wave elastography imaging (SWEI) is a clinically proven method for providing information on the tissue elasticity in addition to morphological ultrasound (US) data. The SWEI principle is based on the shear modulus contrast in the particular tissue. For quantitative shear modulus imaging, most commonly used SWEI techniques rely on the measurement of the shear wave speed (SWS), whereby acoustic radiation force offers a straightforward possibility to combine the creation and the tracking of the shear wave in a single US transducer setup. For time-of-flight SWEI methods, differential arrival times of the shear wave at multiple, laterally offset measurement positions are used to estimate the local SWS.

Against the background of the clinical applicability of SWEI imaging, reducing the SWS estimation error is a primary focus of ongoing research. System-dependent error sources play an important role in impairing the quality of this diagnostic modality and are mainly manifested as variance in the SWS images.

With regard to the origin of errors in the SWS estimates, system-dependent noise can be generally introduced as error of the arrival time measurement, leading to a time delay error, or the measurement of the tracking position. In [1], system-dependent sources of noise in SWEI were systematically examined. There, one of the main sources of error was related to the variance in the displacement estimation. In [2], an analytical formulation was derived, to predict the impact of displacement estimation variance on the arrival time measurements. In turn, the variance of displacement estimates is dependent on the signal-to-noise ratio (SNR) of the radio-frequency (RF) data and is thoroughly discussed for the standard time-delay estimation problem [3], [4].

However, it was observed that SWS images were characterized by noise, even during simulation experiments with perfect RF data SNR. In [5], a correlation between the noise in SWS images and the speckle pattern of the underlying US image was investigated. The origin of speckle is based on constructive and destructive interference from randomly distributed speed-of-sound inhomogeneities which lead to high and low RF signal intensities at specific locations within the imaging field of view due to the convolution with the system's point spread function (PSF). Hence, it is hypothesized that the RF signal does not deterministically originate from the center of the particular PSF. It may also be likely that the RF signal originates from an off-center point, due to the interference pattern. In this way, the measurement position may be shifted towards strong, constructive interferences. The shifted measurement position leads to a delayed or early tracking of the shear wave and thus a shortened or prolonged time delay measurement.

Moreover, the noise in SWEI due to this effect was found to be much more pronounced for multiple-tracking-location approaches, than for approaches using a single track location and multiple excitation pulses [6]. Further, the influence of the adjustable tracking distance regarding the noise in SWS phantom measurements was investigated experimentally in [7]. In [5], this significant noise source was referred to as "speckle bias" but will be termed "speckle effect" for the remainder of this work. This speckle effect was shown to have a major impact on the variance of SWS estimates and thus, on the overall image quality in SWEI. Since the speckle effect is closely related to the parameters of the US imaging system, e.g. the shape and dimension of the PSF, the quality of the SWS images is likely to depend on these parameters.

In this work, the impact of the speckle effect on the quality

This work was funded by the German Federal Ministry of Education and Research, contract number 13GW0069A-B (project SAMBA-PATI).

of the time-of-flight SWEI measurement is quantified using numerical simulations. The investigated US imaging parameters are the shape and dimensions of the imaging PSF, the tracking distance of the time-of-flight reconstruction and the deterministic shear wave speed. Moreover, the impact of axial segment length of the windowed, time domain displacement estimation method is investigated, since information from independent speckle realizations is incorporated in the axial segment of the displacement estimation. The impact on the quality of the SWEI is investigated in terms of the variance on the reciprocal speed data, termed slowness data, since the slowness data is typically used as input for SWEI regression kernels. Moreover, the impact of RF data noise is quantified and compared to the impact of the speckle effect.

II. Methods

A. Simulation of the Shear Wave Field

Simulations of plane shear waves, were realized by solving the 1-D shear wave differential equation numerically. Therefore, a finite differences time domain (FDTD) method was implemented in MATLAB. For the 1-D differential equation, the space-time domain was converted into a discrete space-time grid with $x_r = r \cdot \Delta x_{\mathrm{Sim}}\,, r = 0, 1, ..., R-1$ and $t_l = l \cdot \Delta t_{\mathrm{Sim}}\,, l = 0, 1, ..., L-1$, where x_r is the lateral dimension, $\Delta x_{\mathrm{Sim}} > 0$ is the distance of the discrete points on the lateral axis, t_l is the slow-time and $\Delta t_{\mathrm{Sim}} > 0$ is the sampling period. The Taylor series development at the operating point (x_r, t_l) allows to derive a second order approximation for the displacement $u_r^l = u(x_r, t_l)$ [8]

$$u_r^{l+1} = c_r^2 \frac{\Delta t_{\mathrm{Sim}}^2}{\Delta x_{\mathrm{Sim}}^2}(u_{r+1}^l - 2u_r^l + u_{r-1}^l) + 2u_r^l - u_r^{l-1} \qquad (1)$$

where c_r is the true shear wave speed. For the shear wave excitation, the initial displacement at x_0 was chosen to resemble a typical shear wave in elastography applications [9]. The center frequency was chosen to $350\,\mathrm{Hz}$ and the bandwidth was chosen to $200\,\%$. The displacement magnitude was set to 10 μm. By adjusting c_r, various SWS values could be assigned along the lateral direction leading to homogeneous or inhomogeneous SWS distributions. For the simulations of a 2-D plane shear wave, the 1-D wave simulation was extended in the z-direction by $u(x_r, z_k, t_l) = u(x_r, t_l)$, for $k = 0, ..., K-1$.

B. Simulation of US Data

The US simulations were performed using the US simulation toolbox Field II [10]. Walking aperture beamforming was used in this simulation. For each line of RF data, a subaperture, centered around that RF line, was used. The number of elements in the subaperture as well as the center frequency and the relative bandwidth were varied. A summary of the US imaging parameters is given in table I.

For each set of imaging parameters, simulations of single point scatterers were performed, to validate the dimensions of the resulting PSFs. The PSF dimensions $\sigma_{\mathrm{PSF,x}}$ and $\sigma_{\mathrm{PSF,z}}$ were determined by least-squares fitting a 2-D Gaussian function to the intensity profiles of the single scatterer simulations.

Table I: US Transducer Simulation Parameters

Parameter	Value/ Range
Center frequency f_c	$5-7.8$ MHz
Bandwidth (-6dB)	101.5 %
Sampling frequency f_s	1 GHz
Speed of sound c	1540 m/s
Probe focus	25 mm
Attenuation	none
Element pitch	200 μm
Phantom width x height	5 mm x 10 mm
Size of active aperture	4 mm - 12.8 mm
Sampling period Δt	200 μs
SNR of RF data η_{SNR}	0dB, 15dB, 30dB, $+\infty$

For each set of imaging parameters, 5 independent realizations of scatterer distributions were made. The phantom width and height were set to $5\,\mathrm{mm}$ and $10\,\mathrm{mm}$, respectively. A number of 35 scatterers per resolution cell was used for the simulation, while it has been shown that 11 scatterers per resolution cell is already sufficient to achieve sufficient speckle statistics. The RF signal sampling frequency f_s was set to $1\,\mathrm{GHz}$. The first frame of US data was simulated with the initial spatial distribution of the scatterers. Thereafter, the scatterer positions were displaced by the shear wave field $u(x_r, z_k, t_l)$. Subsequent US frames were simulated with a sampling period of $\Delta t = 200\,\mu\mathrm{s}$. White Gaussian noise of varying noise powers was added to the simulated data, leading to varying SNRs of the acquired RF data.

C. Displacement Estimation

Displacement estimation was performed using 1-D windowed NCC [3]. In order to validate the impact of the axial segment length of the NCC estimation, the segment length N was varied between $2.5\,\lambda$ and $7.5\,\lambda$. For the NCC estimation, the sampling rate f_s was reduced to 200 MHz.

D. Shear Wave Speed and Slowness Reconstruction

For the commonly used time-of-flight reconstruction, the SWS between two lateral positions is calculated based on the arrival times t_i and t_j of the shear wave

$$c_{ij} = \frac{x_j - x_i}{t_j - t_i} = \frac{x_{ij}}{t_{ij}}\,, \quad i = 1:I,\ \ j = 1:I,\ \ i \neq j \qquad (2)$$

$$s_{ij} = \frac{1}{c_{ij}}\,, \qquad (3)$$

where x_i, x_j are lateral positions, x_{ij} is the lateral distance between two positions, t_{ij} is the time delay and c_{ij} is the calculated SWS. The reciprocal speed s_{ij} is termed slowness. The reconstruction was performed in a row-by-row manner.

Prior to time-of-flight reconstruction, the estimated displacement data $\widehat{u}(x_i, t)$ were interpolated along the dimension of

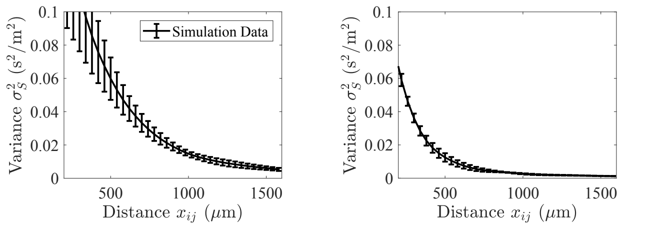

(a) $\sigma_{\mathrm{PSF,x}} = 446\,\mu\mathrm{m}$ (b) $\sigma_{\mathrm{PSF,x}} = 206\,\mu\mathrm{m}$

Figure 1: Variance of slowness estimates σ_s^2 versus tracking distance x_{ij}. Simulation results (black) for varying lateral PSF size $\sigma_{\mathrm{PSF,x}}$. The black line and bars mark the mean and the standard deviation over 5 independent speckle realizations.

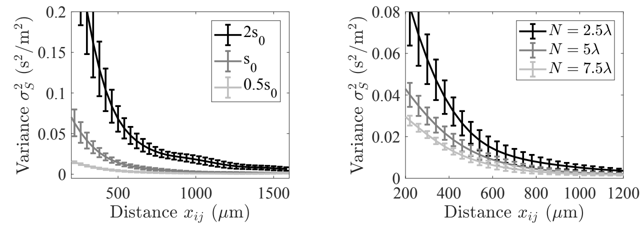

(a) $s_0 = 0.465$ s/m (b) $\sigma_{\mathrm{PSF,x}} = 286\,\mu\mathrm{m}$

Figure 2: (a) Impact of deterministic shear wave slowness on the variance of the slowness estimates. Variance σ_s^2 versus tracking distance x_{ij} for $0.5s_0$, s_0, $2s_0$ ($s_0 = 0.465$ s/m) and $\sigma_{\mathrm{PSF,x}} = 245\,\mu\mathrm{m}$. (b) Impact of the NCC segment length. Variance σ_s^2 versus tracking distance x_{ij} for $N = 2.5\lambda$, 5λ, 7.5λ, $\sigma_{\mathrm{PSF,z}} = 132\,\mu\mathrm{m}$ and $\sigma_{\mathrm{PSF,x}} = 286\,\mu\mathrm{m}$. The lines and bars mark the mean and the standard deviation over 5 independent speckle realizations.

the slow time t, yielding a slow time sampling rate of $1\,\mathrm{GHz}$. Based on the estimated displacement data, the arrival time t_i was determined using

$$t_i = \underset{t}{\mathrm{argmax}}(\widehat{u}(x_i, t))\,. \tag{4}$$

With the determined arrival times the slowness was calculated using (2) and (3). To investigate the impact of the aforementioned parameters, the variance of the distribution of the slowness estimates σ_S^2 was calculated over the entire region of the phantom.

III. Results

A. Variance of Slowness Estimates as Function of the PSF Dimensions

In Fig. 1, the variance of the slowness estimates as function of tracking distance x_{ij} is shown. The simulation results (black line) are shown for lateral PSF sizes $\sigma_{\mathrm{PSF,x}}$ of $446\,\mu\mathrm{m}$ and $206\,\mu\mathrm{m}$, respectively. In general, it can be seen that for small tracking distance the variance of the slowness estimate does not tend to infinity. At large tracking distances, additional tracking distance does not significantly increase σ_s^2. The comparison of Fig. 1.a and 1.b also reveals the impact of the PSF of the imaging system. With reduced lateral PSF size, the overall variance of the slowness estimates is reduced, which becomes particularly apparent for medium tracking distances.

B. Impact of the Shear Wave Speed

The variance of the slowness estimate versus the deterministic shear wave speed is depicted in Fig. 2.a. To maintain a consistent representation, the deterministic speed is expressed as deterministic slowness using (3). The lateral PSF size set to $\sigma_{\mathrm{PSF,x}} = 245\,\mu\mathrm{m}$ and the RF data SNR was set to $\eta_{\mathrm{SNR}} = +\infty$. It can be recognized, that the variance of the slowness estimates increases with the square of the shear wave slowness.

C. Impact of the NCC Segment Length

In Fig. 2.b, the variance of the slowness is plotted versus the tracking distance. The segment length was varied from 2.5λ to 7.5λ with $\sigma_{\mathrm{PSF,x}} = 286\,\mu\mathrm{m}$ and $\sigma_{\mathrm{PSF,z}} = 132\,\mu\mathrm{m}$. In general, the overall variance is reduced with increased axial segment length of the NCC estimation.

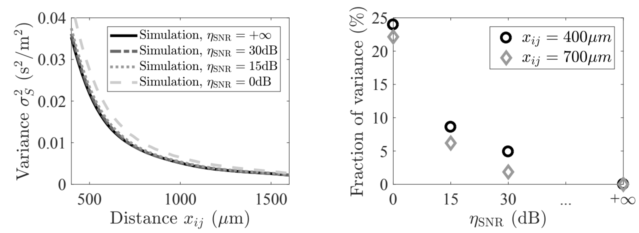

(a) $\sigma_{\mathrm{PSF,x}} = 344\,\mu\mathrm{m}$ (b) $\sigma_{\mathrm{PSF,x}} = 344\,\mu\mathrm{m}$

Figure 3: Impact of RF data noise. (a) Variance σ_s^2 versus tracking distance x_{ij} for $\sigma_{\mathrm{PSF,x}} = 344\,\mu\mathrm{m}$ and varying RF data SNR. (b) Relative share of the total variance due to RF data noise versus RF data SNR for $\sigma_{\mathrm{PSF,x}} = 344\,\mu\mathrm{m}$ and varying tracking distances.

D. Impact of RF data Noise vs. Impact of Speckle Effect

To assess the influence of displacement estimation errors on the variance of the slowness estimates, noise was added to the RF data after the US simulations leading to varying RF data SNRs η_{SNR}. Fig. 3.a shows the variance of the slowness estimates versus tracking distance for varying SNRs. It can be seen that for 15 dB and 0 dB only minor amounts are added to the overall variance of the slowness estimates, compared to the simulation without added noise. In Fig. 3.b, the relative fraction of variance due to RF data noise is shown over varying RF data SNRs. For realistic RF data SNRs the relative fraction does not exceed 10% of the overall variance with the majority of the variance caused by the speckle effect.

E. Impact on the SWS Images

Fig. 4 shows an example of the resulting SWS images, when the straight forward time-of-flight approach in (2) is employed. For the FDTD simulation, the homogeneous SWS was set to $c = 2.25\,\mathrm{m/s}$. Fig. 4.a shows the result of a large imaging PSF ($\sigma_{\mathrm{PSF,x}} = 380\,\mu\mathrm{m}$, $\sigma_{\mathrm{PSF,z}} = 132\,\mu\mathrm{m}$) and Fig. 4.b shows the

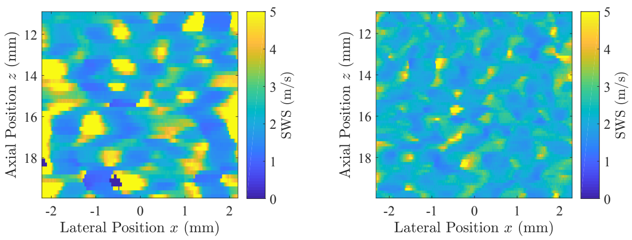

(a) SWS result, $\sigma_{\mathrm{PSF,x}} = 380\,\mu\mathrm{m}$

(b) SWS result, $\sigma_{\mathrm{PSF,x}} = 206\,\mu\mathrm{m}$

Figure 4: Impact of the lateral PSF size on the SWS images. For the FDTD simulation, the homogeneous SWS was set to $c = 2.25\,\mathrm{m/s}$. No noise was added to the RF data ($\eta_{\mathrm{SNR}} = +\infty$). The time-of-flight reconstruction was performed using a fix tracking distance $x_{ij} = 600\,\mu\mathrm{m}$. (a) PSF dimensions: $\sigma_{\mathrm{PSF,x}} = 380\,\mu\mathrm{m}$, $\sigma_{\mathrm{PSF,z}} = 132\,\mu\mathrm{m}$ (b) $\sigma_{\mathrm{PSF,x}} = 206\,\mu\mathrm{m}$, $\sigma_{\mathrm{PSF,x}} = 87\,\mu\mathrm{m}$.

SWS result acquired with a smaller PSF ($\sigma_{\mathrm{PSF,x}} = 206\,\mu\mathrm{m}$, $\sigma_{\mathrm{PSF,z}} = 87\,\mu\mathrm{m}$). The SWS results of the large PSF show more noise, compared to the results acquired with the small PSF. Moreover, lower spatial frequencies can be seen in the SWS images in Fig. 4.a which correlate with the larger PSF dimensions.

IV. Discussion

For the simulations in III-A to III-C and III-E, no noise was added to the RF data and the impact of the speckle effect could be investigated in isolation. With a decreased lateral dimension of the PSF, the over all variance of the slowness estimates was reduced (see Fig. 1). A larger PSF size also correlated with lower spatial frequencies of the noise distribution in the SWS images (see Fig. 4) which is in line with the findings in [5].

In Fig. 2, it can be seen that the variance of the slowness estimates scales quadratic with the deterministic slowness s_0. For these investigations, the variance of the slowness estimates was of primary interest, since slowness estimates are typically used as input for averaging kernels. However, if the SWS is calculated directly from the slowness estimates, the distribution of the slowness estimates will be transformed through the non-linear function as the slowness is the reciprocal of the SWS. The variance of the SWS estimates is therewith a function of σ_S^2 and additionally, a function of s_0. For large s_0 and small σ_S^2 the transform can be linearly approximated and the variance of the SWS estimates σ_C^2 may be obtained by scaling σ_S^2.

The results in Fig. 2.b show that the segment length of the displacement estimation has an impact on the variance of the slowness estimates, also when RF data noise is excluded from the simulation. Here, US data from a number of PSFs are included in the axial segment for the NCC estimation, leading to an averaging of the respective position errors and thus to a reduction of the resulting position error of the displacement estimate. The benefits of reducing the position error during the displacement estimation using partially uncorrelated information from a 2-D neighborhood were investigated in [11].

In III-D, noise was added to the RF data leading to varying SNRs. Here, even a moderate to strong addition of noise showed only a minor impact on the overall variance with a maximum share of 10 %.

These results indicate that the speckle effect is a major contributor to the deterioration of SWS images and that the speckle effect can be reduced by setting the investigated imaging parameters accordingly.

V. Conclusions

The speckle effect is a fundamental disturbance in time-of-flight shear wave imaging setups. This contribution provides insight into the relationship between the variance of slowness estimates and US imaging parameters such as the lateral and axial dimensions of the PSF. Moreover, the impact of the segment length of the displacement estimation scheme, the lateral tracking distance during time-of-flight reconstruction, the deterministic shear wave speed and the SNR of the RF data were investigated. The results provide a basis for an improved understanding of how speckle corrupts the SWS estimation.

References

[1] Y. Deng, N. C. Rouze, M. L. Palmeri, and K. R. Nightingale, "On system-dependent sources of uncertainty and bias in ultrasonic quantitative shear-wave imaging," *IEEE Trans. Ultrason., Ferroelectr., Freq. Control*, vol. 63, no. 3, pp. 381–393, 2016.

[2] T. Deffieux, J.-L. Gennisson, B. Larrat, M. Fink, and M. Tanter, "The variance of quantitative estimates in shear wave imaging: theory and experiments," *IEEE Trans. Ultrason., Ferroelectr., Freq. Control*, vol. 59, no. 11, pp. 2390–2410, 2012.

[3] W. F. Walker and G. E. Trahey, "A fundamental limit on delay estimation using partially correlated speckle signals," *IEEE Trans. Ultrason., Ferroelectr., Freq. Control*, vol. 42, no. 2, pp. 301–308, 1995.

[4] T. Ersepke, T. C. Kranemann, and G. Schmitz, "On the performance of time domain displacement estimators for magnetomotive ultrasound imaging," *IEEE Trans. Ultrason., Ferroelectr., Freq. Control*, vol. 66, no. 5, pp. 911–921, 2019.

[5] S. A. McAleavey, L. O. Osapoetra, and J. Langdon, "Shear wave arrival time estimates correlate with local speckle pattern," *IEEE Trans. Ultrason., Ferroelectr., Freq. Control*, vol. 62, no. 12, pp. 2054–2067, 2015.

[6] P. J. Hollender, S. J. Rosenzweig, K. R. Nightingale, and G. E. Trahey, "Single-and multiple-track-location shear wave and acoustic radiation force impulse imaging: matched comparison of contrast, contrast-to-noise ratio and resolution," *Ultrasound Med. Biol.*, vol. 41, no. 4, pp. 1043–1057, 2015.

[7] K. Offerdahl and S. McAleavey, "Influence of transmit beamforming parameters on image quality in quantitative elastography," in *Proc. IEEE Int. Ultrason. Symp. (IUS)*. IEEE, 2017, pp. 1–5.

[8] U. S. Inan and R. A. Marshall, *Numerical electromagnetics: the FDTD method*. Cambridge University Press, 2011.

[9] T. Shiina *et al.*, "Wfumb guidelines and recommendations for clinical use of ultrasound elastography: Part 1: basic principles and terminology," *Ultrasound Med. Biol.*, vol. 41, no. 5, pp. 1126–1147, 2015.

[10] J. A. Jensen, "Field: A program for simulating ultrasound systems," in *Med. Biol. Eng. Comput.*, vol. 34, suppl. 1, pt. 1, 1996, pp. 351–353.

[11] T. Ersepke, T. C. Kranemann, and G. Schmitz, "2-d bayesian displacement estimation improves contrast-to-noise/resolution trade-off in shear wave elasticity imaging," in *Proc. IEEE Int. Ultrason. Symp. (IUS)*, 2019.